Journal of Volcanology and Geothermal Research 353 (2018) 83–94

Contents lists available at ScienceDirect

Journal of Volcanology and Geothermal Research

journal homepage: www.elsevier.com/locate/jvolgeores

Crustal seismicity associated to rpid surface uplift at Laguna del Maule Volcanic Complex, Southern Volcanic Zone of the Andes

Carlos Cardona [a,c], Andrés Tassara [b,c,d,*], Fernando Gil-Cruz [a], Luis Lara [a], Sergio Morales [a], Paulina Kohler [b], Luis Franco [a,c]

[a] Observatorio Volcanológico Chileno, Servicio Nacional de Geología y Minería, Rudecindo Ortega 03850, Temuco, Chile
[b] Departamento de Ciencias de la Tierra, Universidad de Concepción, Victor Lamas 1290, Concepción, Chile
[c] Programa de Doctorado en Ciencias Geológicas, Universidad de Concepción, Victor Lamas 1290, Concepción, Chile
[d] Millenium Nucleus The Seismic Cycle at Subduction Zones, Minecon-ICM, Chile

ARTICLE INFO

Article history:
Received 4 May 2017
Received in revised form 5 December 2017
Accepted 15 January 2018
Available online 31 January 2018

Keywords:
Rhyolitic volcano system
Large-scale deformation
Repetitive seismic swarms
Cross correlation wave form

ABSTRACT

Laguna del Maule Volcanic Complex (LMVC, Southern Andes of Chile) has been experiencing large rates (ca. 30 cm/yr) of surface uplift as detected since 2008 by satellite geodetic measurements. Previous works have modeled the source of this deformation as an inflating rectangular sub-horizontal sill underlying LMVC at 5 km depth, which is supposedly related to an active process of magmatic replenishment of a shallow silicic reservoir. However little is known about the tectonic context on which this activity is taking place, particularly its relation with crustal seismicity that could help understanding and monitoring the current deformation process. Here we present the first detailed characterization of the seismic activity taking place at LMVC and integrate it with structural data acquired in the field in order to illuminate the possible connection between the ongoing process of surface uplift and the activation of crustal faults. Our main finding is the recognition of repetitive volcano-tectonic (VT) seismic swarms that occur periodically between 2011 and 2014 near the SW corner of the sill modeled by InSAR studies. A cross-correlation analysis of the waveforms recorded for these VT events allows identifying three different seismic families. Families F1 and F3 share some common features in the stacked waveform and its locations, which markedly differ from those of family F2. Swarms belonging to this later family are more energetic and its energy was increasing since 2011 to a peak in January 2013, which coincide with maximum vertical velocities detected by local GPS stations. This points to a common process relating both phenomena. The location of VT seismic swarms roughly coincides with the intersection of a NE-SW lineament with a WNW-ESE lineament. The former shows clear field evidences of dextral strike-slip that are fully consistent with one nodal plane of focal mechanism for well-recorded F2 events. The conjugate nodal plane of these focal mechanisms could coincide with the WNW-ESE lineament, for which our field reconnaissance suggests a dominant normal motion. Events belonging to families F1 and F3 are also dominantly strike-slip but with some mixture with thrust and normal components. Our results, in conjunction with results of previous authors, suggest a complex mechanical interaction between the arrangement of crustal faults forming the structural framework on which the magmatic plumbing system of LMVC is emplaced and the inflating source at depth.

1. Introduction

Laguna del Maule Volcanic Complex (LMVC; Fig. 1) is one of the most hazardous active volcanic systems on Southern Andean volcanic zone (Singer et al., 2014) as suggested by the combination of an impressively large volume of Holocene silicic volcanism (Hildreth et al., 2010; Andersen et al., 2017) and large rates of current surface uplift detected by satellite geodetic measurements (Fournier et al., 2010; Feigl et al., 2014; Singer et al., 2014; Le Mével et al., 2015, 2016). Preliminary work shown by Singer et al. (2014) indicates that this current deformation is related to seismically active faulting at shallow depth. In this contribution we present the first detailed characterization of the seismic activity taking place at LMVC and integrate it with structural data acquired in the field in order to illuminate the ongoing process of surface uplift.

LMVC comprises 36 rhyolite and rhyodacite coulees and domes that erupted during the Holocene from 24 separated vents surrounding a 9 × 11 km lake (Fig. 1). These silicic products lies on top of more than one hundred pre-Holocene vents from which ca. 350 km^3 of intermediate to acidic lavas and pyroclastic rocks were erupted since 1.5 Ma

* Corresponding author at: Departamento de Ciencias de la Tierra, Universidad de Concepción, Victor Lamas 1290, Concepción, Chile.
E-mail address: andrestassara@udec.cl (A. Tassara).

https://doi.org/10.1016/j.jvolgeores.2018.01.009
0377-0273/

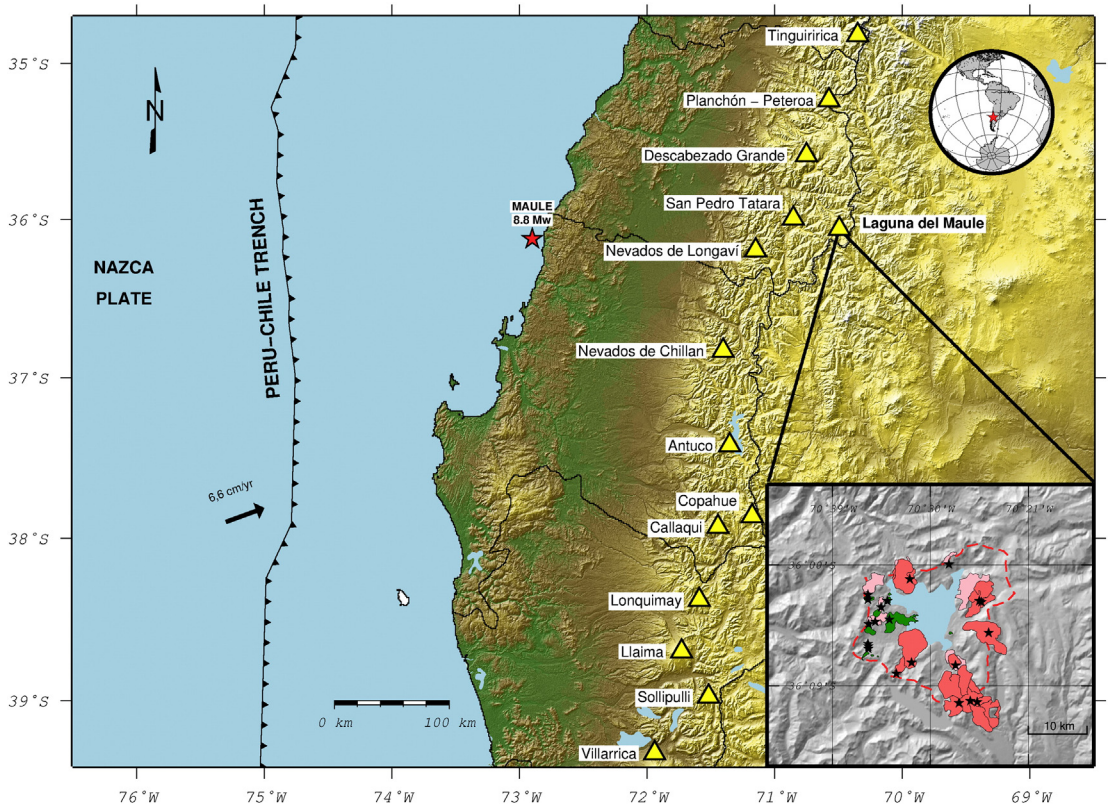

Fig. 1. Tectonic setting of Laguna del Maule Volcanic Complex (LMVC). Shaded relief topographic image showing the location of the Southern Andes Volcanic zone with yellow triangles being volcanoes under surveillance by OVDAS, the epicenter of the Mw = 8.8 27-Feb-2010 Maule earthquake (red star). Inset shows a simplified geological map (adapted from Hildreth et al., 2010) pf LMVC, showing the 36 postglacial lava flows and domes (pink = rhyolites; light pink = rhyodacites; green = andesites) that are surrounding the volcanic complex, the black stars are the volcanic vents and the red discontinuous line represents the rim of the basin.

(Hildreth et al., 2010; Singer et al., 2014). Part of this activity was related to episodes of caldera-forming eruptions (Hildreth et al., 2010), some of them likely occurring during the Holocene (Andersen et al., 2017). Although no historic eruptions are associated to LMVC, the described geological setting implies an important volcanic hazard for this region, which is amplified by the ongoing surface uplift episode that has been recognized using the Interferometric Satelite Aperture Radar (InSAR) method (Fournier et al., 2010; Feigl et al., 2014; Singer et al., 2014; Le Mével et al., 2015, 2016). An interferogram between 2003 and 2004 analyzed by Fournier et al. (2010) indicated no detectable deformation, but a clear inflation signal with maximum 18.5 cm/yr line of sight (LOS) deformation centered on the lake basin appears in an InSAR image for 2007–2008. These authors modeled this surface deformation as caused by a shallowly dipping rectangular sill located 5 km below the lake and opening at rates of 60 cm/yr. Interferograms analyzed by Feigl et al. (2014) indicated LOS deformation rates exceeding 28 cm/yr at the surface between 2007 and 2012, and confirmed the inflating sill at 5 km depth as the most likely deformation source. Further studies combining InSAR with local GPS data published by Le Mével et al. (2015) show that the uplift rate achieved its maximum just before the Mw8.8 February 2010 Maule great subduction earthquake and that this rate decreased again in January 2013 to stabilize around 20 cm/yr until at least mid-2014. Le Mével et al. (2016) developed numerical models of magma injection to analyze the temporal evolution of surface deformation. They suggest that between 2007 and 2009 the injection pressure rise to a maximum of 11.5 MPa with a volume flow rate of 1.3 m^3/s, which then decreased to 0.7 m^3/s in 2014 and keeps decreasing until 2016. As data analyzed in our contribution started to be recorded in 2011, we must recall that our results will help to characterize the seismic activity occurring during the declining phase of upper crustal inflation associated with decreasing magma injection pressure into the magmatic reservoir underneath LMVC.

Given the indirect evidences of volcanic unrest available by the end of 2010, the Observatorio Volcanologico de los Andes del Sur (OVDAS; the Chilean Volcano Observatory depending on the Geological Survey SERNAGEOMIN) decided to deploy seismic and continuous GPS instruments to monitor LMVC. This network started recording data in April 2011 confirming the large uplift rates and showing clear evidence of shallow seismic activity surrounding the inflating zone.

The goal of this contribution is to present the first systematic characterization of the seismic activity recorded by the local OVDAS network at LMVC between 2011 and 2014. After describing the network, data and methods, we first show the different types of seismic events that can be recognized through a classification scheme. Then we describe the temporal evolution of these events, which allows recognizing the repetitive occurrence of seismic swarms at the SW extreme of the inflating source. We then show the spatial distribution of relocated seismicity along with the 1D seismic velocity model resulting from the relocation process. For seismicity occurring in the region of the swarms we present a cross correlation waveform analysis that allows the identification of different seismic families and the resulting focal mechanisms for a number of these well-located events. Finally we integrate these results with those derived from a structural mapping of the LMVC in order to establish a possible connection of the recorded seismicity with the current surface deformation.

2. Seismic network, data and methods

During April 2011 OVDAS deployed a surveillance network composed by 5 portable 30 s Guralp broadband (BB) stations, installed around the volcanic complex at distances between 0 and 9 km from

the center of the deforming zone. First seismic records showed clear evidence of shallow seismicity and therefore OVDAS installed a telemetric communication system during austral summer 2012 in order to transmit data in real time to the observatory. During this field campaign 3 dual-frequency continuous GPS stations were also installed close to the deformation zone. A year later (February 2013) the network was improved with the installation of other 2 Guralp 30 s BB seismometers and 2 additional GPS stations. Between February and April 2014, a temporary seismic network composed by 5 portable Guralp BB stations was deployed in order to improve the azimuthally coverage and to obtain accurate seismic locations. The network is complemented with 10 additional 30 s and 120 s BB seismometers, installed previously on neighboring volcanoes. In summary (Fig. 2), between April 2011 and October 2014 a monitoring network composed by 21 BB stations and 5 dual-frequency continuous GPS stations was consolidated.

Here we consider continuous seismic records from April 2011 to October 2014 (~3.5 years). A first preliminary processing level over these data was applied as part of the routinely monitoring task at OVDAS. This considers the manual recognition of individual events from the continuous seismic signal and extraction of basic information for each of them as amplitude, duration, energy, wave phases and preliminary seismic location. This preliminary processing recognized >3200 volcanic seismic events of shallow depth (<8 km) related to the internal dynamic of LMVC. A second, post-processing level was implemented in this work with the aim to refine the location and characterization of the recognized seismicity. This includes following procedures.

2.1. Seismic events classification

The seismic signals related to each recognized event was classified following Lahr et al. (1994) and Chouet (2003), which is based on the waveform appearance on the seismic records, as well as additional elements that help to discern about its seismic source. Thus, we established three main kinds of volcanic signals: volcano-tectonic events (VT) related to brittle fracturing of rocks induced by magmatic activity, long period events (LP) that suggest a genesis related to fluids movement or pressures changes of volcanic conduits, and tremor signals (TR) which origin are similar to LP events, but with a sustained excitation through the time that can last by hours or days.

2.2. Seismic location methods and crust model determination

Using as a starting point a database of 1060 preliminary located events, we performed a relocation process using the Join Hypocenter Determination (JHD) algorithm (Crosson, 1976; Ellsworth, 1977; Thurber, 1983). For this, the local crustal velocity model was refined using VELEST (Kissling et al., 1994) considering only the 163 events having the best quality (gap < 180°, ERH and ERZ > 2.0 Km). As initial model we used the 1D model proposed by Bohm et al. (2002) for the central part of Chile. Our model is divided in 20 horizontal layers of 1 km thickness. We divided the procedure into three phases: 1) we relocated the preliminary earthquakes, fixing the velocities distribution suggested by Bohm et al. (2002), and a new epicenter distribution was obtained, as well as the delays for each seismic station and the error of the solution. This procedure was done iteratively to reach the best solution with low error that better represented the P and S phases observed. 2) The epicenters were fixed and the velocity for each layer was varied iteratively in order to find the 1D crust model velocity distribution with the lower error. 3) With the new 1D velocity model the hypoDD method (Waldhauser and Ellsworth, 2000) was applied to minimize the errors and improve the accuracy of the epicenter distribution.

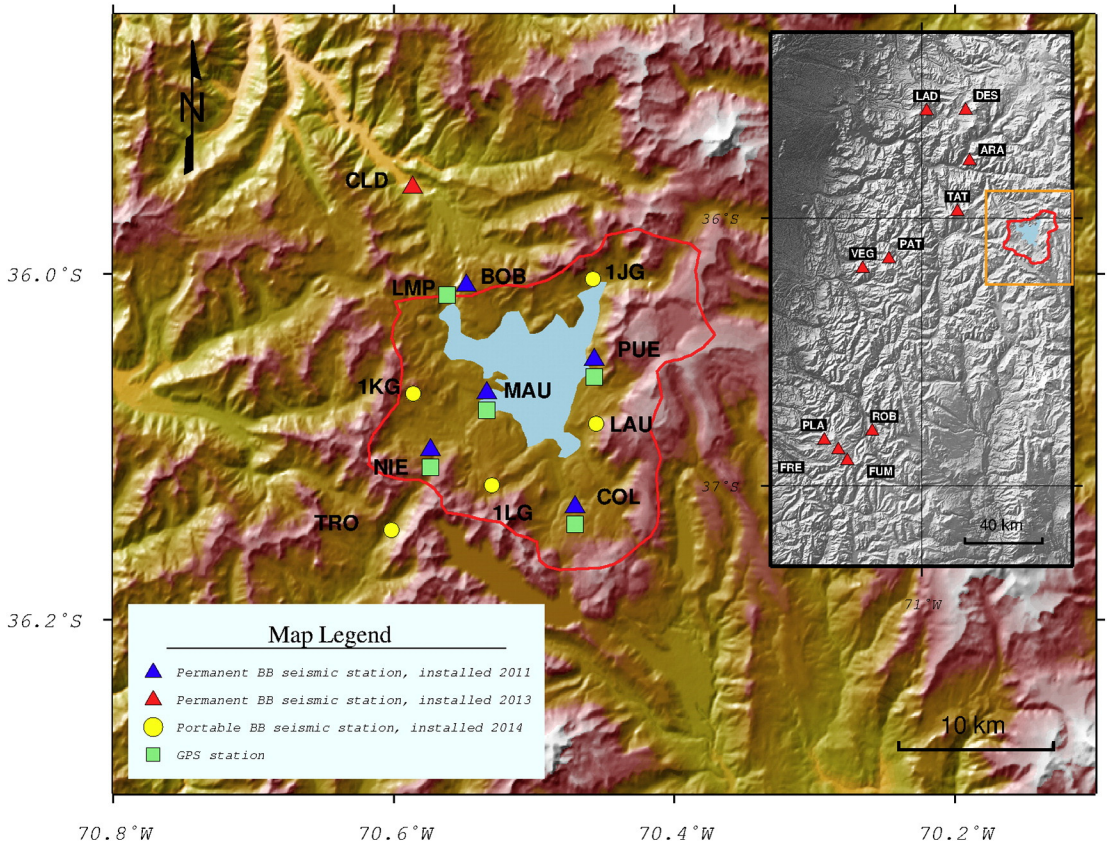

Fig. 2. Distribution of seismic stations composing the LMVC seismic network used in this study. The main figure shows the 11 stations deployed inside the lake basin, whereas the inset shows locations of other 10 stations deployed by OVDAS on neighbors volcanoes. The red line shows the rim of the volcanic basin.

2.3. Seismic swarms determination and cross-correlation analysis

Cross-correlation analysis is a method commonly used in seismological studies with the aim to determine the degree of similitude between waveforms of a seismic dataset (Poupinet et al., 1984). This allows recognizing seismic families or multiplets in a specific region, which makes possible an analysis of its recurrence, time progressions and spatial distributions. Correlation studies have been applied successfully to autodetect and classify seismic events, improving for instance locations of small magnitudes events (Shelly et al., 2013). Autodetection of events as based in waveform correlation has been specifically effective in cases where there is a high rate of events productivity in short lapse time, as seismic swarms (Shelly et al., 2007). As we show below, a series of seismic swarms can be recognized from seismic records of the LMVC zone. With the aim to evaluate the waveform similitude between each seismic swarm, a cross-correlation analysis was done, searching to establish temporal variations of the waveforms included into each swarm episode. For this we isolate each seismic event and choose 5 sec since the P wave time arrive, after a Butterworth bandpass filter (0.5–15 Hz) was applied. The Cross Correlation Function (CCF) compares the seismic signal between pair of events, with CCF values between 0 and 1, being 1 the maximum similitude value. In our case, events with correlation coefficients higher than 0.7 were included into a same seismic family.

2.4. Seismic energy

We computed the seismic energy for each seismic swarm with the aim to provide a meaningful physical magnitude for comparison between discrete seismic episodes. To compute seismic energy E_t we used the approach proposed by Boatwright (1980), assuming the media as an isotropic elastic homogeneous half space:

$$E_t = 2\pi\rho_s V_p d^2 \int A^2 \Delta_t$$

where, A = sum of seismic amplitude of the entire seismic swarm record. ρ_S = solid density. V_p = P wave velocity. d = distance between seismic source to reference station. Δ_t = delta time of calculation.

For this analysis, we choose NIE as the reference station because it is the closest one to the swarm source (2 km from seismic swarm source).

2.5. Focal mechanism determination

To obtain the focal mechanism solutions we used the FOCMEC software package (Snoke et al., 1984) included into SEISAN program (10.1 version). This tool uses the first P wave polarities of a given set of stations, search all possible plane fault solutions that better represent the distribution of polarities into the focal sphere, search iteratively the strike, dip and rake for the two nodal planes that well separated the compressive and distensive polarities, assuming a pure double couple moment tensor. We selected those events with a well-constrained seismic location, at least 10 observations, and good azimuthal distribution of the stations. We only allow two (over ten) polarity errors in order to guarantee a good constraint of the focal mechanism solution.

3. Results

3.1. Classification of seismic activity

We applied the classification criteria for volcanic events suggested by Lahr et al. (1994) and Chouet (2003) to continuous seismic records obtained during April 2011 and December 2014 at station NIE. From a total of 3218 preliminarily recognized events related with the dynamic of the volcanic system, 2568 of them were classified as volcano-tectonic (VT) events (80% of the total sample), 362 as long-period (LP) events (11% of the sample) and 279 as tremor pulses (9% of the sample). This shows a clear tendency of the volcanic system to generate seismicity related with the brittle fracturing of crustal material (Fig. 3).

A prominent aspect of the seismic activity detected at LMVC, which is notable in the daily number of recorded seismic events (Fig. 3), is the periodic occurrence (every 2 to 3 months in average) of swarms of VT events. We define a swarm as a group of >50 events occurring during less than 1 h. Using this criteria, swarm episodes are formed by a number between 63 and 300 seismic events of local magnitude between 0.1 and 2.2 occurring in restricted time spans of 25 to 180 min. Each of the 14 swarms recognized here are marked by vertical arrows in Fig. 3, whereas Table 1 presents some characteristic parameters for each episode.

The seismic activity related with the dynamics of fluids (LP and TR), shows a low level of occurrence compared with VT events, with average values of <1 event/day, low velocity amplitudes (0.5–2 μm/s) and reduced displacement lower than 2 cm^2. It was possible to obtain the location of one relatively large (M_L = 1.3) LP event. This occurred in

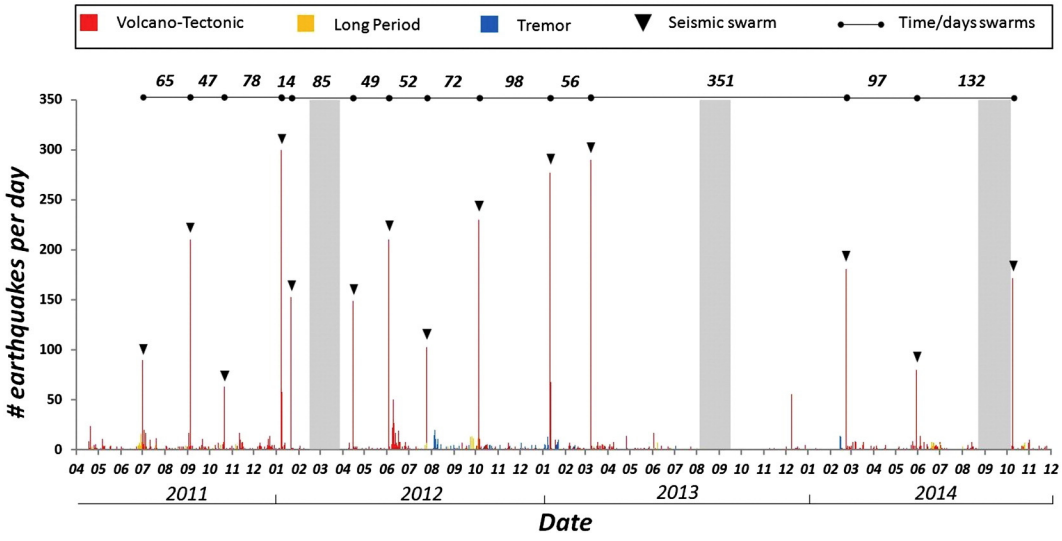

Fig. 3. Temporal evolution of volcano seismicity as recorded at station NIE. Graph shows number of earthquakes per day for the entire study period, recognizing different types of events (volcano-tectonic in red, long period in yellow, and tremor in blue). Inverted black triangles denote occurrence of swarms of volcano-tectonic events. Numbers at the top of the figure shows amount of days between swarms. Grey bars indicate gaps in data record.

Table 1
Quantitative parameters of VT seismic swarms occurred in the LMVC.

Episode	Date dd-mm-yy	Number of events	Duration (minutes)	M_L Max	Energy (10^8 J)	Time between swarms (days)
1	01-Jul-11	90	25	1.2	0,9	–
2	04-Sep-11	210	90	1.9	2,7	65
3	21-Oct-11	63	160	1.5	0,6	47
4	07-Ene-12	300	167	1.8	13,4	78
5	21-Ene-12	153	180	1.4	1,1	14
6	15-Abr-12	149	70	1.7	5,9	85
7	03-Jun-12	210	160	2.2	68	49
8	25-Jul-12	103	55	1.2	0,6	52
9	05-Oct-12	230	180	1.7	13,9	72
10	11-Ene-13	277	180	1.9	155,7	98
11	08-Mar-13	290	150	1.7	2,3	56
12	22-Feb-14	181	170	0.9	0,5	351
13	30-May-14	80	30	1.0	0,8	97
14	09-Oct-14	172	100	2.1	4,2	132

February 20th 2014 (2 days before swarm number 12) and recorded clear P-wave arrivals at 10 stations. The determined epicenter is located near of the SW vertex of the area suggested as the source of surface deformation by the InSAR studies (Fig. 5). Due to the low energy of the rest of the LP seismicity, locations could not been determined. However the distribution of amplitudes associate with these events in the stations where they are mostly observed (MAU and NIE) suggests that most of the LP seismicity is generated in the same area. The spectrums of this type of seismicity have frequencies between 1 and 5 Hz with a dominant peak around 3 Hz (Fig. 4). This frequency distribution was observed in all stations, suggesting that it corresponds to sources frequencies. However, it was not possible to characterize this type of seismicity with a greater detail.

3.2. 1D velocity model and seismicity relocation

We use P- and S-phases readings of the preliminary located seismicity to derive a local 1D seismic velocity model with Velest (Kissling et al., 1994). Table 2 shows the obtained P-wave and S-wave velocity model and compared it against the regional velocity model of Bohm et al. (2002), which was the starting model for the iterative inversion. We note that our model has smaller P-wave velocities than the regional model, mostly between 0 and 5 km depth where the difference is larger than 1 km/s (5.5 km/s for Bohm et al., 2002 compared to 4.4 km/s in our model). This difference is expected since the regional model was constructed for an area located 500 km southward of LMVC characterized by a crystalline plutonic basement of the volcanic arc that contrast with mostly volcano-sedimentary rocks forming the basement of LMVC.

Table 2
P and S velocity model and Vp/Vs ratio of 1D velocity model obtained in this work compared with the regional model of Bohm et al. (2002).

	This work			Bohm et al. (2002)		
Depth (km)	V_p (km/s)	V_s (km/s)	V_p/V_s	V_p (km/s)	V_s (km/s)	V_p/V_s
−3	4,31	2,28	1,89	4,39	2,40	1,83
1	4,39	2,69	1,63	4,39	2,40	1,83
2	4,46	3,06	1,46	5,51	3,19	1,73
5	5,65	3,20	1,77	6,28	3,60	1,74
15	6,00	3,47	1,73	6,28	3,60	1,74
20 (fixed)	6,89	3,93	1,75	6,89	3,93	1,75
35 (fixed)	7,40	4,15	1,78	7,40	4,12	1,80
45 (fixed)	7,76	4,35	1,78	7,76	4,55	1,71
55 (fixed)	7,94	4,46	1,78	7,94	4,55	1,75
90 (fixed)	8,34	4,69	1,78	8,34	4,77	1,75

Based on this new velocity model, we applied JHD (Crosson, 1976; Ellsworth, 1977; Thurber, 1983) and HypoDD (Waldhauser and Ellsworth, 2000) to relocate the seismicity. Fig. 5 shows the distribution of the epicenters, with seismicity concentrated in several clusters that can be associated with different possible sources. The first cluster is located in the western region of the studied area and is related to a relatively large (Mw = 6.2) crustal earthquake occurred in June 6th 2012 and its aftershock sequence, composed by nearly 600 events. NEIC and GCMT catalogs reported a dextral strike-slip focal mechanism along a NNE fault plane, consistent with our own solution based on first P-wave motion at 17 stations.

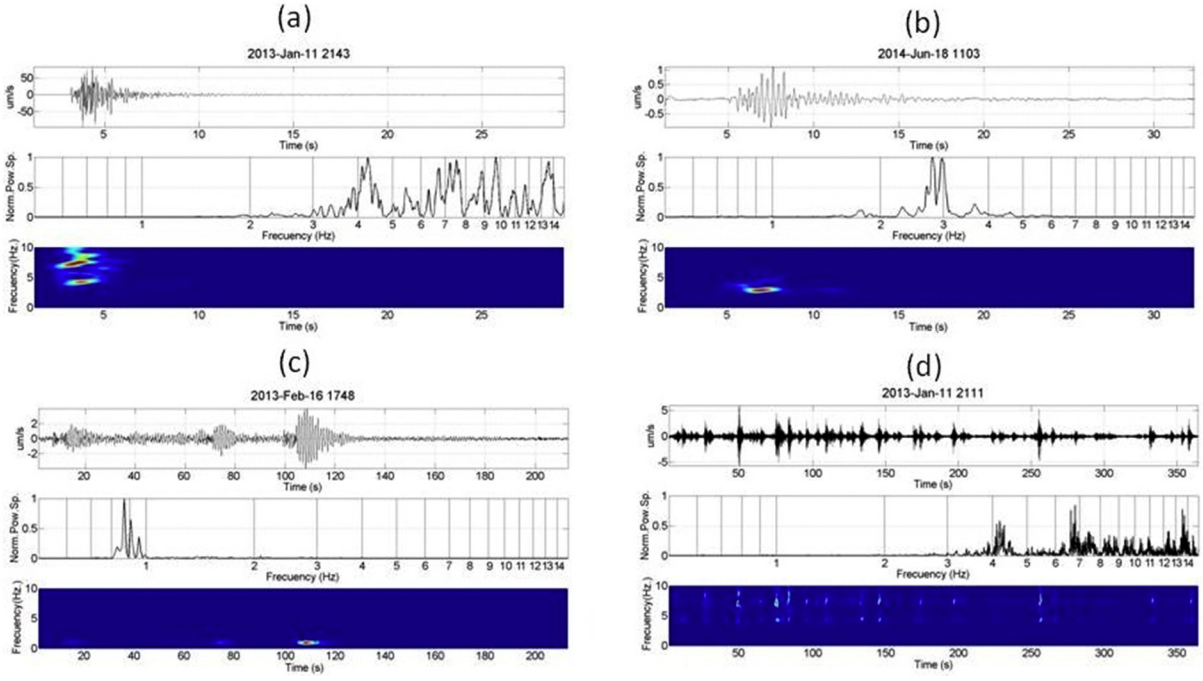

Fig. 4. Examples of seismic records. For each subfigure we show the complete waveform (upper panel), frequency spectrum and spectrogram. a) typical volcano-tectonic (VT) event belonging to seismic swarms, b) long period (LP) event, c) tremor (TR), and d) portion of a VT seismic swarm. VT events like in a) present signals with frequencies between 1 and 20 Hz, while the LP and TR events present a narrow band with frequencies lower than 4 Hz.

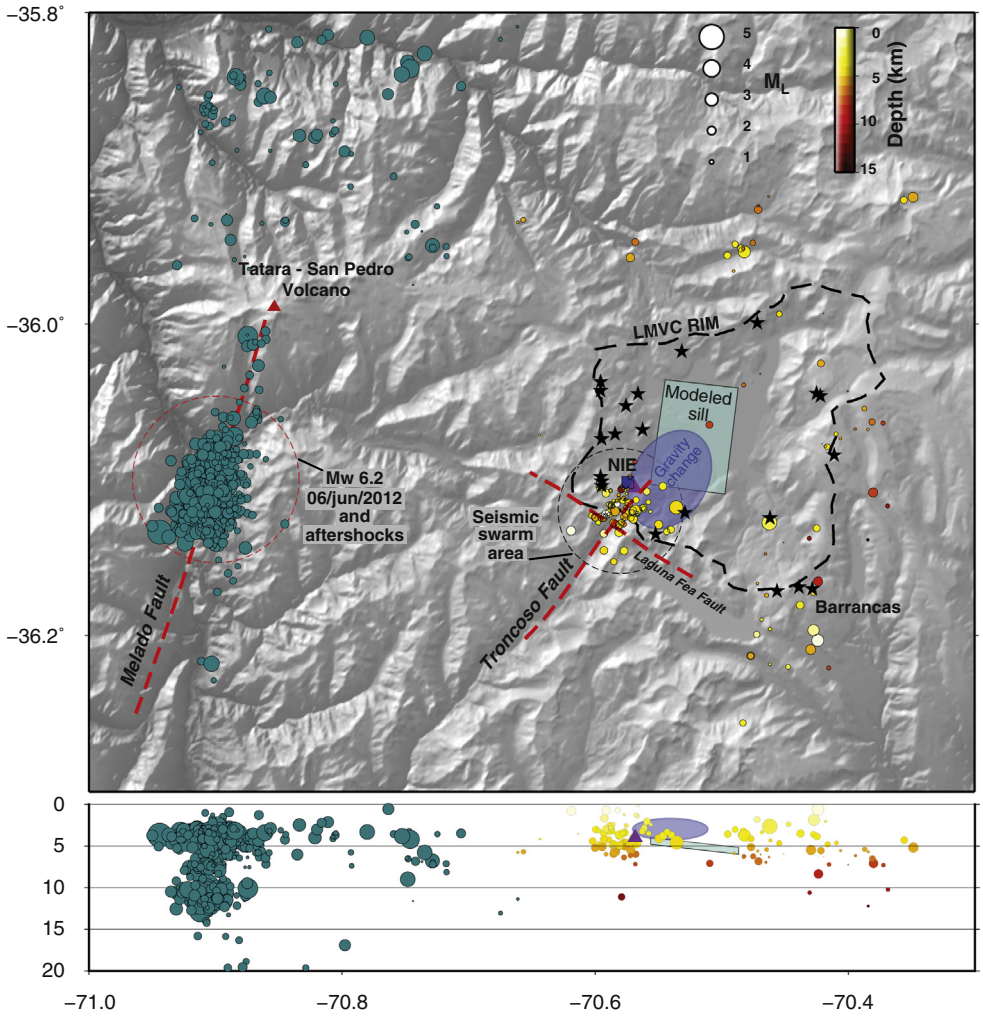

Fig. 5. LMVC seismic location map between April 2011 and December 2014. Red dashed circle marks the location of a tectonic earthquake Mw = 6.2 occurred in June 6th of 2012 and the sequence of ~600 aftershocks (green circles scaled by magnitude) along the Mellado fault that intersects the Tatara-San Pedro Volcano (red triangle). Volcano-tectonic events surrounding LMVC are color-coded by depth and scaled by magnitude. Black starts are volcanic centers with recognized Holocene activity (Hildreth et al., 2010) A cluster of seismicity is located around the intersection of two main topographic lineaments (Troncoso and Laguna Fea Faults). Another cluster of seismic activity does occur near volcanic center Barrancas at the SE border of the basin. Purple triangle on the seismic swarm area shows the location of an energetic LP event. Blue square shows the reference seismic station 'NIE'. Green rectangle represent the sill modeled by InSAR and GPS data (Fournier et al., 2010 and Feigl et al., 2014) and the blue ellipsoid shows the zone where Miller et al. (2016) reported an excess mass by microgravity measurements.

A NNE-oriented nodal plane is suggested by the alignment of aftershocks in this direction, coinciding with the orientation of a regional structure that we call here Melado Fault (Fig. 5). Lupi and Miller (2014) suggest that this earthquake and its aftershocks could be related to static stress transfer from the Mw = 8.8 Maule 2010 earthquake toward a crustal fault.

The source area of the repetitive seismic swarms described in Section 3.1 is located in the SW sector of the complex, with hypocenters fluctuating between 2 and 5 km depth. This area coincides with the SW vertex of the sill modeled as the source of InSAR-observed surface deformation (Fournier et al., 2010; Feigl et al., 2014; Le Mével et al., 2015), and with a zone where Miller et al. (2016) reported mass changes recognized by microgravity measurements during 2013 and 2014. Furthermore, the area of the swarms corresponds to a notable structural intersection (as described below) and is characterized by the presence of centers of postglacial rhyolitic emissions (Hildreth et al., 2010). Similarly, a cluster of seismicity located in the SE extreme of the lake basin is closely related to one of the most active rhyolitic volcanic centers (called Barrancas by Hildreth et al., 2010), where Andersen et al. (2017) recognized at least 13 eruptive phases during the last 2.5 My.

3.3. Cross correlation of VT swarms episodes

We performed a correlation waveforms analysis using cross correlation functions (CCF) that focused on seismicity related to the VT swarms at the SW region of the complex. We took those events with S-P arrival times <1.5 s at NIE reference station. Fig. 6 shows the distribution matrix of cross correlation values obtained applying the CCF algorithm to the 450 events grouped in 14 swarms. This analysis allows us to recognize the level of similarity between events belonging to each swarm and between different swarms, being useful for the identification of families of swarms as characterized by a high level of correlation between them. The inspection of Fig. 6 suggests that 13 swarms can be grouped in 3 different families. Family F1 is composed by swarms E1, E8 and E13; family F2 is the most numerous and includes swarms E2, E4, E7, E9, E10 and E14; and family F3 with swarms E3, E5, E11 and E12. Swarm E6 has one of the strongest auto-similarity between events belonging to the same swarm but shows very little similarity with the other 13 swarms grouped into the recognized families. A detailed inspection of Fig. 6 allows suggesting that E6 could be potentially related to family F2.

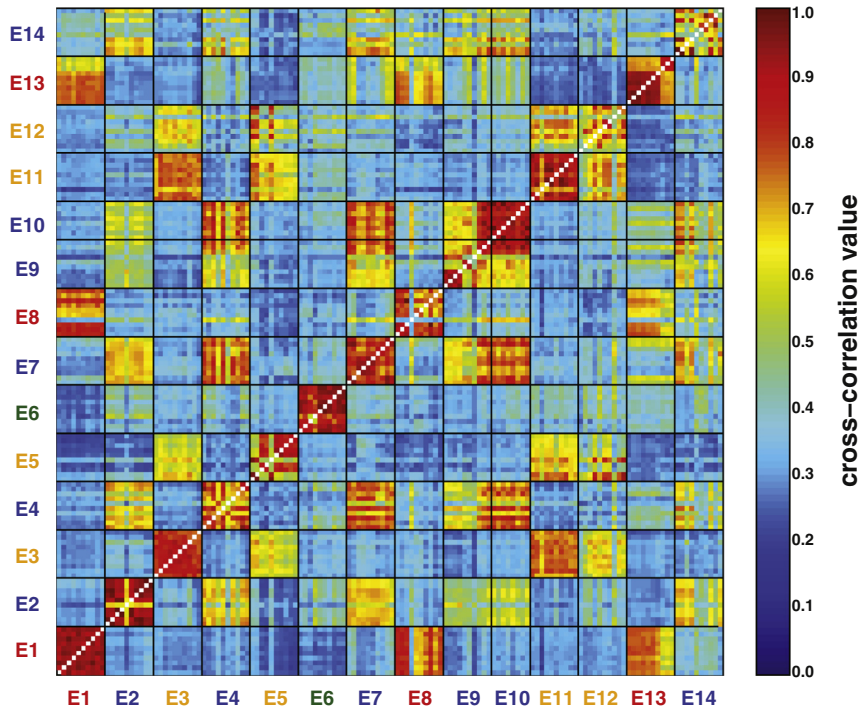

Fig. 6. Matrix showing the correlation values computed for all events belonging to seismic swarms. Warm/cold colors represent high/low correlations values. The alphanumeric code below and at the left hand of the figure represent each one of the fourteen recognized seismic swarm episodes. The colors of the alphanumeric code represents families; red is for family 1 (F1) including swarms E1, E8 and E13; blue is for family 2 (F2) including E2, E4, E7, E9, E10 and E14); orange is for family 3 (F3) including swarms E3, E5, E11 and E12; and green is for the isolated swarm episode E6.

We used the matched-filter technique to obtain the stacking of all the events included in each family by normalizing the amplitude and filtering the signals to a common reference (as used for instance at Villarica Volcano by Richardson and Waite, 2013). Fig. 7 shows the stacked waveform for the three recognized families allowing a comparison of amplitude and phase for direct and coda waves of the seismic signals. This analysis shows that each family is characterized by a given temporary correspondence in scale of the amplitude and arrival time of the direct phases, mostly for the first 4 s after arrival of the P wave.

In addition, the comparison between the stacked waveform for each family shows differences on S-P values (<0.3 s). Family 2 has the larger S-P of ~0.7 s, followed by Family 1 with S-P of ~0.5 s and Family 3 with S-P of ~0.4 s. These differences are explained by variation in the distance between the specific location of the source of each seismicity family and the references station NIE. In addition, we note that the stacked waveform of families F1 and F3 are suggestively similar one to each other (mostly within 2 s after the arrival of the S wave) with much more high frequency energy than the one observed for family F2. These observations could indicate that F1 and F3 are rupturing relatively

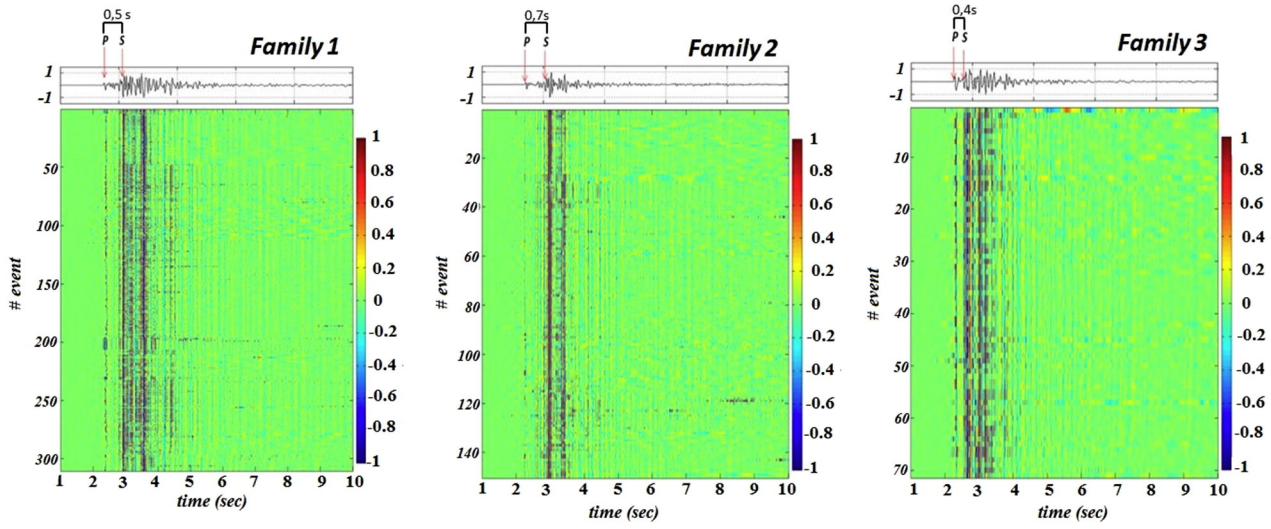

Fig. 7. Stacking of volcano-tectonic events as grouped by the corresponding family. The stacked signals are for the vertical component at seismic station NIE. To apply the matched filter technique, the amplitudes of events were normalized between 1 (red) and −1 (blue) and a standard butterwort band pass filter was applied (0.2–12 Hz). Note the stability of the direct phase and the differences of the S-P values between families (shown at the top of each panel), suggesting differences in the location of the each family.

closer patches of the same fault with similar frictional properties, and that these notably differ from the properties of another fault being ruptured by family F2.

3.4. Temporal evolution of swarms

We analyze now how the recognized seismic swarms evolved in time. Fig. 8 shows the number of events composing each swarm, duration of the swarm, maximum local magnitude (from Table 1) and total seismic energy (computed as explained in Section 2.4). We first note that all these parameters are roughly correlated one to each other (with the exception of the duration for the first 5 swarms), and then we concentrate in describing temporal variations of calculated energy, which should be more clearly related with the physical phenomena behind these swarms. We recall that our study period began in 2011, i.e. 4 years after the start of the inflation process recognized by InSAR studies, so we are analyzing a snapshot that did not capture either the beginning of the event or any dynamic effects that might have followed the 2010 Maule earthquake.

We note that the energy of the swarms sequence as a whole (i.e. independent of its family) was gradually increasing from relatively low values in July 2011 to a maximum in January 2013 (swarm E10). After this, the next swarm was notably less energetic and afterwards no swarms were recorded for nearly a year (although a gap in data recorded by the seismic network between August and September 2013 could perhaps masks another swarm?). In February 2014, a low-energy swarm (E12) marked a re-start of swarm activity, which continued with other two swarms during this year with smoothly increasing energies.

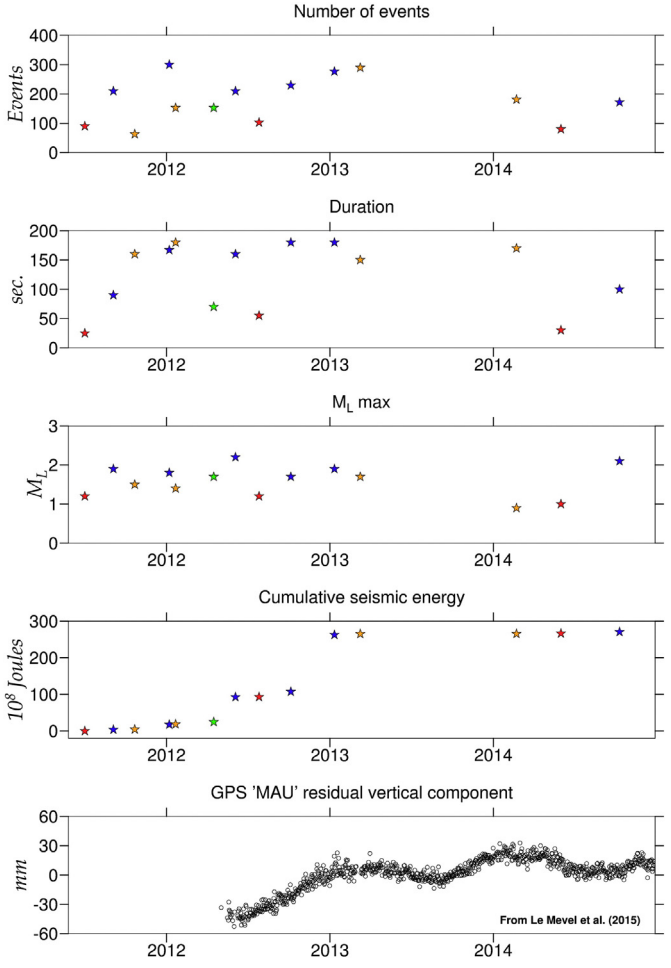

Fig. 8. Temporal evolution of VT swarm's parameters during the study period. Colors for each swarm represent families as in Fig. 6. The X axis format is 'month-year'. Family F2 (blue points) contains the most energetic seismic swarms. The graphs below shows the variation of deformation rates from 2012 to 2014 extracted from the Le Mével et al. (2015), note that during April 2012 and January 2013 when the deformation rates were increasing the cumulative energy rise due to the most energetic swarm episodes were recorded.

The evolution of the cumulative energy with time is interestingly related with a more or less clear shift in the activity of the three recognized seismic families. The episodes related to swarm included into family 2, usually demark large increases of the cumulative energy. As each family is likely related to the repetitive rupture of an individual and isolated seismogenic fault patch, this observation suggests certain degree of mechanical interaction between these isolated patches, as discussed below. Also interesting is to note (Table 1 and Fig. 8) that swarms belonging to families F1 and F3 had always energies lower than 1.1×10^8 J (with the exception of swarm E11 of family F3 that occurred just after the maximum release of energy associated to swarm E10 in January 2013, see Table 2). Swarms of family F2 were always more energetic than this threshold marking all the cumulative energy leaps in Fig. 8. The similar behavior of families F1 and F3 in terms of released energy and their notable difference with family F2 is complementary to observations revealed by the cross-correlation analysis of Section 3.3. A phase to remark occurred between April 2012 and January 2013: at this time the cumulative energy has the larger leap observed that temporally matches with a period reported by Le Mével et al. (2015) where the deformation rates were increasing (see Fig. 8.). Additionally, Miller et al. (2016) reported mass changes recognized by microgravity measurements between during 2013 and 2014, calculating a decrease of residual gravity of 124 ± 12 microGals.

3.5. Focal mechanism and field evidence for the source of the seismic swarms

The improvement of the seismic network in January 2014 occurred mostly around the region where the swarms were previously detected (Fig. 2), with the aim of refining their location and to solve their focal mechanisms. During 2014, three swarms (one for each family) were recorded, allowing a better location of events than those registered before this year, and the computation of focal mechanisms by P-wave first motion method for several relatively large events. A total of seventeen focal mechanisms were solved and are shown in Fig. 9 along with their epicenter location. Three well-located events of swarm E14 (family F2) are grouped near the intersection of a clear SW-NE topographic lineament coinciding with Cajón de Troncoso valley and a more diffuse WNW-ESE lineament parallel to the orientation of Laguna Fea (Fig. 9). Focal mechanisms of this swarm are dominated by a strike-slip motion that is compatible with either dextral sense along a SW-NE structure or sinistral sense along the WNW-ESE lineament. By the other hand, events belonging to swarms E12 (family F3) and E13 (family F1) are clustered 2–3 km westward of the location of swarm E14 along the continuation of the WNW-ESE lineament and at constant depth of 4–5 km. The three focal mechanisms obtained for events of swarm E13 are almost purely strike-slip with nodal planes rather similar to those computed for E14. Focal mechanisms for events of E12 (6 in total) show a more heterogeneous character both in its kinematics (mix of strike-slip, normal and reverse motion) and orientation of nodal planes, although with a dominance of directions similar to the other two swarms. Fig. 9 also shows other 3 events also located along the WNW-ESE lineament but toward the east of its intersection with the NE-SW Troncoso lineament. The epicenter of these events coincides with the emission vent of Las Nieblas rhyolitic flow, one of the most recent (<2 ka) postglacial eruptive products (Singer et al., 2014). Focal mechanisms of these quakes are similar to those of E14 and E12 but with a significant normal component along a NE-SW plane.

With the aim of exploring the structural character of topographic lineaments concentrating the activity of seismic swarms, we performed a field reconnaissance of the area surrounding the intersection of the

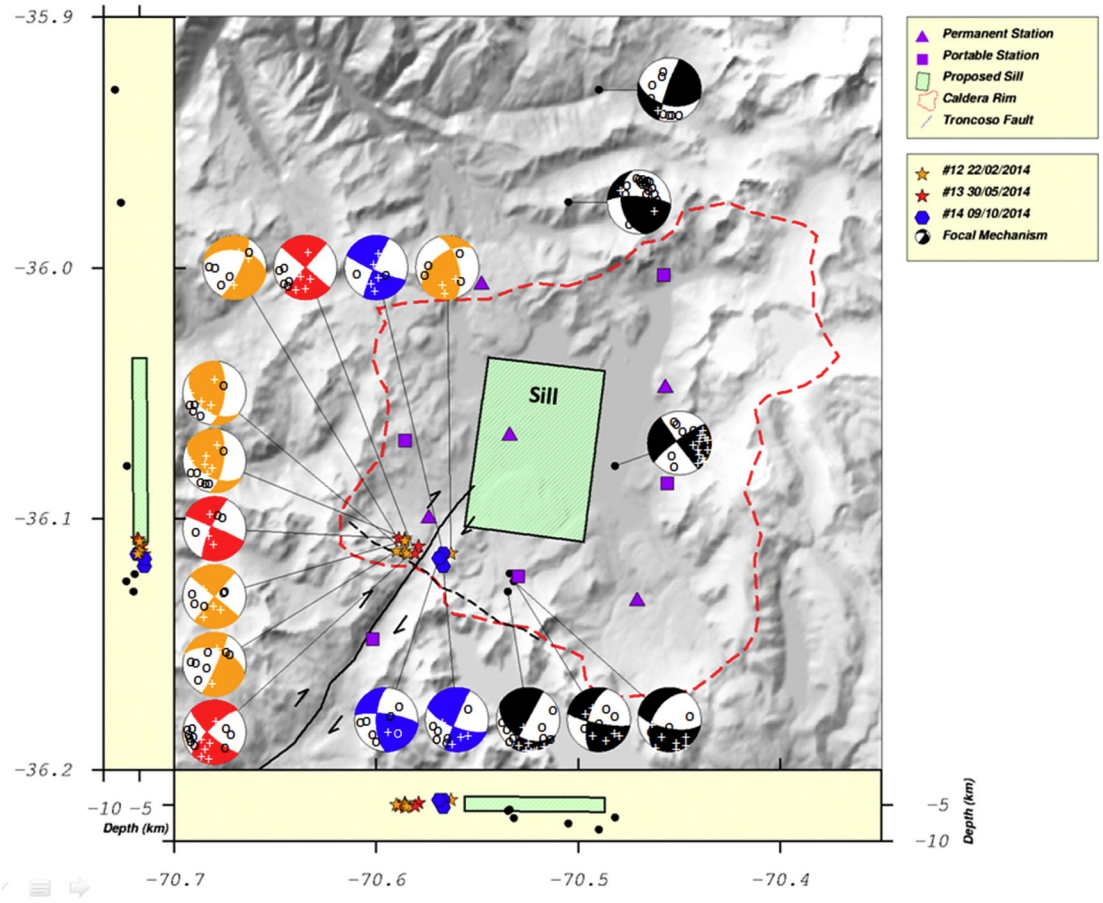

Fig. 9. Focal mechanisms and locations for 18 well-located VT events recorded by the full seismic network operative during 2014. Colors of events denote seismic families as in Fig. 6. Focal mechanisms show polarities with 'o' for distensive motion and '+' for compressive motion. The green rectangle represents the location of the sill modeled by InSAR studies.

Troncoso lineament with the WNW-ESE lineament (Fig. 10). Along the southern prolongation of the former, the basement of the LMVC (volcano-clastic and intrusive rocks of Oligo-Miocene age) is affected by brittle faulting expressed as sub-horizontal striation parallel to the valley (Fig. 10D and E), which corroborates that Troncoso is not only a morphologic lineament but a real fault. Integrating structural measurements at observed fault planes along the Troncoso fault, we obtain a fault solution remarkable similar to the dominant focal mechanisms of swarms, i.e. almost pure strike-slip along a NE-SW plane of dextral motion or WNW-ESE plane of sinistral motion. We prefer the first alternative because of the regional orientation of the fault, and suggest that at least those events belonging to E14 are likely rupturing the northern prolongation of the Troncoso fault. However, these events do occur at the intersection of this fault with the WNW-ESE lineament, along which we found morphological evidence of normal faulting along a roughly EW plane (Fig. 10G) and subvertical striation at several fault planes (Fig. 10F). The integrated fault plane solution resulting from these structural data (Fig. 10C) shows a more heterogeneous deformation that is dominated by a normal motion along a WNW-ESE plane with a weak component of strike-slip. Although the kinematics of this fault solution is only roughly compatible with computed focal mechanisms, we think that events located near the vent of Las Nieblas flow and those of swarms E12 and E14 are likely related to this WNW-ESE structure, being less clear its relation with swarm E14.

4. Discussion and conclusion

The most prominent feature of crustal seismicity recognized by our study as accompanying the large inflation episode evidenced at LMVC by InSAR studies (Fournier et al., 2010; Feigl et al., 2014; Le Mével et al., 2016), is the existence of short (0.5 to 3 h long) seismic swarms composed by tens to hundreds of small-magnitude ($ML < 2.2$) quakes recurring every 2–3 months (in average) near the SW corner of the lake basin. The waveform correlation analysis that we applied to the recorded swarm seismicity allows recognizing three different seismic families which activity alternate over the 3.5 years period of this study (Fig. 6). Two of these families (F1 and F3, labeled with red and orange color, respectively in Fig. 7, Figs. 9 and 11) share some significant features, like certain similarity of their stacked waveform, their relatively low energy and their hypocentral location (for well-recorded events) along a WNW-ESE lineament showing field evidence of normal faulting, although computed focal mechanisms are more consistent with strike-slip motion of this fault (mostly for F3, see Fig. 9). Family F2 (labeled with blue color in Fig. 7, Figs. 9 and 11) by the other hand has a distinctive stacked waveform with larger S-P arrival times, larger integrated energy of the swarms and a location at the intersection of the WNW-ESE lineament with the NE-SW Troncoso fault. Strike-slip focal mechanisms for F2 events are consistent either with sinistral motion along the WNW-ESE fault or dextral motion along the Troncoso fault (Fig. 9), which fits with the structural evidence recognized in the field (Fig. 10).

Into this context our main finding is to discover that the SW corner of the sill proposed as source of surface uplift by geodetic studies (Feigl et al., 2014; Le Mével et al., 2015, 2016) roughly coincides with a seismically active structural intersection where a complex spatio-temporal interaction between both faults seems to be likely activated by the inflation of the proposed sill. We discuss here how these phenomena could be causatively connected.

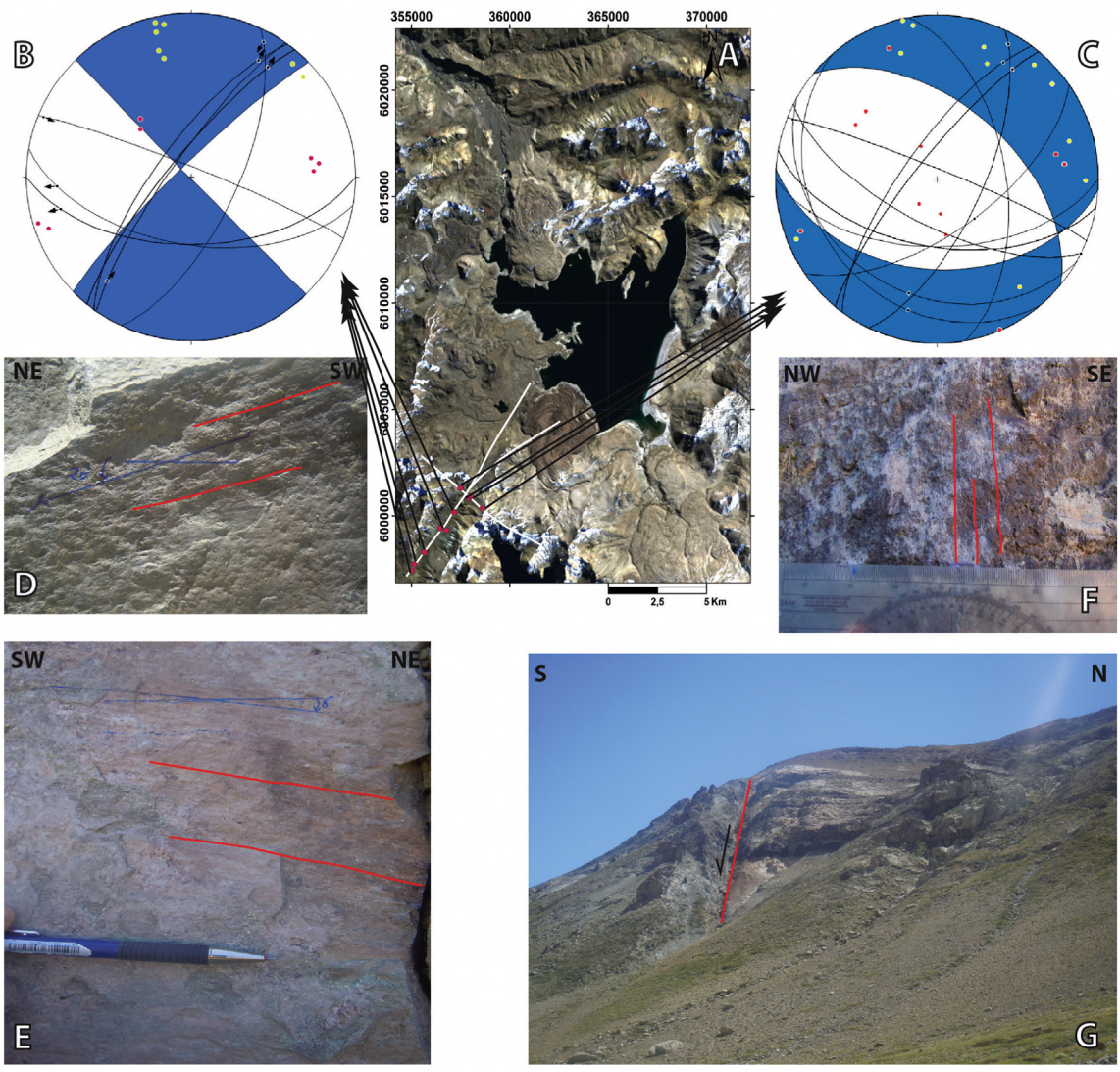

Fig. 10. Field recognition of structures near the region of the VT seismic swarms. A) Satellite image of LMVC showing the location of structural observations (red points) and associated topographic lineaments (white lines). B) Strain diagram showing the best double-couple fault plane solution fitting data acquired at different sites along the NE-SW Troncoso Fault. C) Strain diagram showing the best double-couple fault plane solution fitting data acquired at different sites along the WNW-ESE lineament. D) and E) photographs of outcrops exhibiting evidences of sub-horizontal estriae at Troncoso fault evidencing dominant strike-slip motion. F) photograph of outcrop exhibiting evidence of sub-vertical estriae near WNW-ESE fault suggesting dominant vertical motion. G) photograph of the WNW-ESE lineament suggesting normal motion of the structure.

Swarms of volcano-tectonic (VT) seismic events have been long described at siliceous volcanic complexes like Laguna del Maule. The pioneer work of Hill (1977) proposes that this type of repetitive seismic activity does occur in fault-controlled systems with a critical combination of fluid injection into the faults and changes in the level of regional stress loading the fault system. Rapid deformation of the upper crust by the inflation of the magma reservoir below LMVC can transfer stresses to the structural framework of the volcanic system, as also proposed for other volcanic complexes (Karymsky Volcanic Group, Walter, 2007; Mt. Etna, Feuillet et al., 2006; Cerro Negro, Díez et al., 2005). Into this model, the mechanical interaction between active shallow faults loaded by tectonic stresses and the inflationary source atop the magma reservoir promote the generation of crustal seismicity, eventually triggering the cyclic rupture of frictional asperities along different faults. The periodic alternation between swarms belonging to families F1 and F3 by one side and those of family F2 by the other (Fig. 8) suggests that certain degree of interaction does exist between the fault segment generating F1 and F3 along the WNW-ESE structure and the asperity associated with swarms of family F2 at the intersection of this fault with the Troncoso fault. It seems possible that the activity of a swarm in one fault can transfer stresses to the other fault, adding to those continuously loaded by the inflation of the magmatic source.

Le Mével et al. (2015, 2016) noted a coincidence between the moment when the uplift rate recorded at GPS stations near the center of the inflation region starts decreasing in January 2013 and the occurrence of the largest seismic swarm. Our results confirm that this swarm, E10 belonging to family F2 (Fig. 8), was the most energetic of the entire sequence recorded between 2011 and 2014. Moreover, it seems apparent that before E10, the energy of F2 swarms was gradually increasing, whereas F1 and F3 swarms keep always at lower energies (see Table 1 and Fig. 8). This suggests to us that the seismogenic asperity associated with F2 would be more strongly coupled to the inflation source than those related to F1 and F3, which activity could be seen as a secondary response of the fault system to the primary mechanical interaction between the inflating sill and the fault intersection located close to its SW corner.

A complementary mechanism to explain the repetitive nature of seismic swarms (as also envisaged by Hill, 1977) is the possible interaction of the fault frame with a confined, highly-pressurized hydrothermal system.

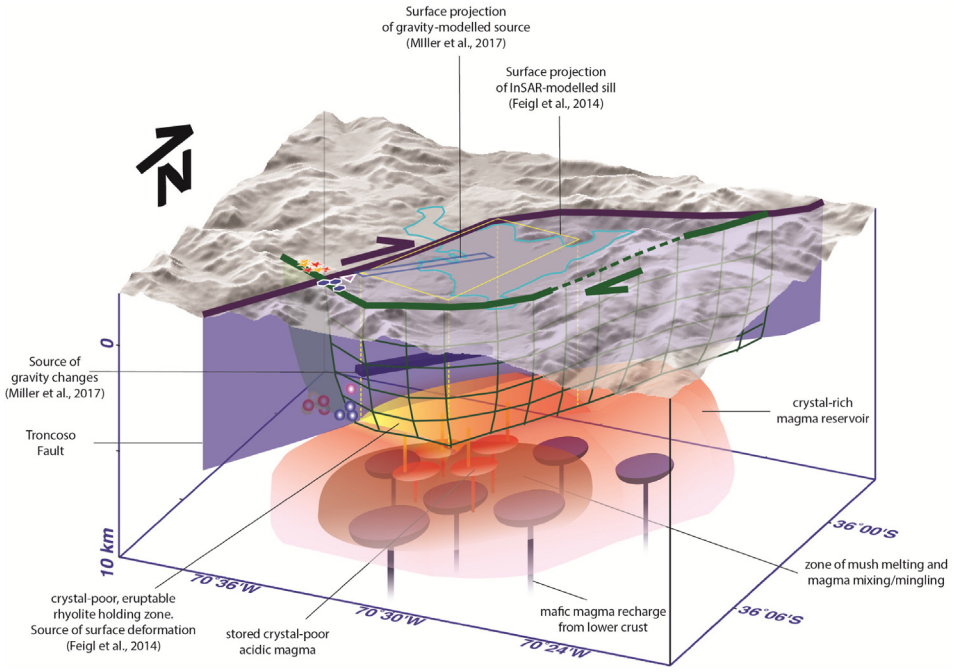

Fig. 11. 3D conceptual model explaining the relationship between crustal structure and magmatic plumbing system underneath Laguna del Maule Volcanic Complex. Hypocenter of seismic swarms recognized in our study are shown as spheres and their epicenters at the surface are marked with symbols and colors of seismic families as defined in Figs. 7 and 9. These seismic swarms are located at the intersection of Troncoso fault with an ENE-oriented lineament (family F2, blue) and along this latter lineament (families F1 and F3). Troncoso fault forms the western structural limit of a NE-SW oriented dextral pull-apart basin, at which base is located the sill modeled as the source of surface uplift imaged by InSAR (Feigl et al., 2014). This in turn coincides with the roof of an extensive magmatic reservoir (as imagined by Andersen et al., 2017) where crystal-poor eruptable rhyolitic magma is likely being cumulated. The scheme also includes the prismatic source of gravity changes proposed by Miller et al. (2017), which SW tip coincides with the SW corner of the inflating sill and roughly with the epicenter of an energetic LP event (purple triangle at the surface) above the hypocenters of F2 swarm.

VT seismic swarms in other rhyolitic systems like Yellowstone and Long Valley (Shelly et al., 2013; Massin et al., 2013) have been related with the episodic rupture of faults as it shear strength decreases once pore pressure reach a certain threshold due to the constant fluid injection at high pressure from a deeper hydrothermal reservoir. This mechanism could be also applicable to swarms recorded in LMVC, moreover after considering that the region of the swarms (mostly for F2) coincides with the epicenter of the recognized LP activity (commonly associated with the movement of fluids). Supporting this idea, temporal gravity changes documented by Miller et al. (2017) have been interpreted as a consequence of hydrothermal fluids circulating in an arrange of NE-SW oriented faults modeled as elongated tabular prisms (Fig. 11) whose SW tip roughly coincides with location of seismic swarms.

Our field evidence of dextral strike-slip brittle faulting along the Troncoso fault coinciding with focal mechanisms of the energetic seismic family (F2) located at it trace, helps to constrain a regional structural model of the LMVC useful to understand the interaction of the deep source of surface deformation with the fault system. We schematize this model in Fig. 11 summarizing all the relevant results that have been recently published for LMVC. We favor a structural model with Troncoso fault as the western master fault of a SW-NE oriented dextral pull apart basin, as also suggested by Miller et al. (2016) based on the relation between the fault and location of a low density anomaly recognized from modeling gravity data. Similar models considering transtensional tectonic regimes associated with pull apart basins along strike-slip structural systems have been proposed for Central Andean Mio-Pliocene calderas (Riller et al., 2001), the Taupo volcanic zone (Spinks et al., 2005), large caldera systems in California including Long Valley (Riley et al., 2012) and Ilopango Caldera in Salvador (Saxby et al., 2016). We think that the base of such tectonically-controlled pull-apart basin can serve as the roof of the magmatic reservoir, as schematized in Fig. 11. This scheme considers the structure proposed by Andersen et al. (2017) for the magmatic plumbing system under LMVC that integrated its temporal and geochemical evolution. This includes a large, long-lived crystal rich reservoir that is sporadically intruded by mafic recharge from the lower crust and develops internal mush zones of magma mingling, mixing and hybridization from which crystal-poor, rhyolitic eruptable magma can be extracted and cumulated in an upper holding zone. This latter zone in our scheme coincides with the base of the pull-apart basin and with the source region of surface uplift. This model as applied to LMVC could allow to clarify the observed synchronicity between rapid surface uplift as produced by magmatic intrusion and/or hydrothermal pressurization at the base of the pull-apart basin with seismic activity of the master fault bounding the basin. Exploring this model requires a detailed correlation analysis of surface deformation and seismic activity aided by modeling stress transfer between different sources, something that we are facing for a future contribution.

Acknowledgements

This research has been partially funded by Observatorio Volcanologico de los Andes del Sur (OVDAS) belonging to Sernageomin (National Geological Survey), US NSF grants EAR-1322595 and EAR-1411779 with Brad Singer (University of Wisconsin-Madison) as PI, and Chilean Fondecyt project 1151175 (Andres Tassara as PI). The Concepción University supports the first author providing a doctoral student grant. We would like to thank to the OVDAS electronic team and specially the electronic engineer Christian Delgado to participate in the fieldwork seismological deployment and the regular service of the seismic stations, and the seismological team of OVDAS to support the authors performing the primary processing of the seismic data. Most figures were generated using GMT software by Wessel and Smith (1991).

References

Andersen, N.L., Singer, B.S., Jicha, B.R., Beard, B.L., Johnson, C.M., Licciardi, J.M., 2017. Pleistocene to Holocene growth of a large upper crustal rhyolitic magma reservoir beneath the active laguna del Maule volcanic field, central Chile. J. Petrol. 2017 (58, 1): 85–114. https://doi.org/10.1093/petrology/egx006.

Boatwright, J., 1980. A spectral theory for circular seismic sources: simple estimates of source dimension, dynamic stress drop, and radiated seismic energy. Bull. Seismol. Soc. Am. 70 (1), 1–27.
Bohm, M., Luthb, S., Echtler, H., Asch, G., Bataille, K., Bruhn, C., Rietbrock, A., Wigger, P., 2002. The Southern Andes between 36° and 40°S latitude: seismicity and average seismic velocities. Tectonophysics 356, 275–289.
Chouet, B., 2003. Volcano seismology. Pure Appl. Geophys. 160, 739–788.
Crosson, R.S., 1976. Crustal structure modeling of earthquake data, 1, simultaneous least squares estimation of hypocenter and velocity parameters. J. Geophys. Res. 81, 3036–3046.
Díez, M., La Femina, P.C., Connor, C.B., Strauch, W., Tenorio, V., 2005. Evidence for static stress changes triggering the 1999 eruption of Cerro Negro Volcano, Nicaragua and regional aftershock sequences. Geophys. Res. Lett. 32 (L04309). https://doi.org/10.1029/2004GL021788.
Ellsworth, W.L., 1977. Three-dimensional structure of the crust and mantle beneath the island of Hawaii. Ph D Thesis. MIT, Massachussetts, USA, p. 1977.
Feigl, K.L., Le Mével, H., Ali, S.T., Córdova, L., Andersen, N.L., DeMets, C., Singer, B.S., 2014. Rapid uplift in Laguna del Maule volcanic field of the Andean Southern Volcanic zone (Chile) 2007–2012. Geophys. J. Int. 196 (2):885–901. https://doi.org/10.1093/gji/ggt438.
Feuillet, N., Cocco, M., Musumeci, C., Nostro, C., 2006. Stress interaction between seismic and volcanic activity at Mt Etna. Geophys. J. Int. 2006 (164):697–718. https://doi.org/10.1111/j.1365-246X.2005.02824.x.
Fournier, T.J., Pritchard, M.E., Riddick, S.N., 2010. Duration, magnitude, and frequency of subaerial volcano deformation events: new results from Latin America using InSAR a global synthesis. Geochem. Geopshys. Geosyst. 11 (1), 1–29 19 January 2010.
Hildreth, W., Godoy, E., Fierstein, J., Singer, B., 2010. Laguna del Maule Field. Eruptive history of a quaternary basalt-to-rhyolite distributed volcanic field on the Andean range crest in central Chile. Boletin No 63, 2010. Subdirección Nacional de Geología. Sernageomin, p. 145.
Hill, D.P., 1977. A model for earthquake swarms. J. Geophys. Res. 82, 1347–1352.
Kissling, E., Ellsworth, W.L., Eberhart-Phillips, D., Kradolfer, U., 1994. Initial reference models in local earthquake tomography. J. Geophys. Res. 99 (19′635–19′646).
Lahr, J.C., Chouet, B.A., Stephens, C.D., Power, J.A., Page, R.A., 1994. Earthquake classification, location and error analysis in a volcanic environment: implications for the magmatic system of the 1989–1990 eruptions at Redoubt Volcano, Alaska. J. Volcanol. Geotherm. Res. 62 (1–4), 137–151.
Le Mével, H., Feigl, K.L., Cordova, L., DeMets, C., Lundgren, P., 2015. Evolution of unrest at Laguna del Maule volcanic field (Chile) from InSAR and GPS measurements, 2003 to 2014. Geophys. Res. Lett. 42, 6590–6598.
Le Mével, H., Gregg, P.M., Feigl, K.L., 2016. Magma injection into long-lived reservoir to explain geodetically measured uplift: application to the 2004–2014 episode at Laguna del Maule volcanic field, Chile. J. Geophys. Res. 121, 6092–6108.
Lupi, M., Miller, S.A., 2014. Short-lived tectonic switch mechanism for long-term pulses. Solid Earth 5 (13–24):2014. https://doi.org/10.5194/se-5-13-2014.
Massin, F., Farrell, J., Smith, R.B., 2013. Repeating earthquakes in the Yellowstone volcanic field: implications for rupture dynamics, ground deformation, and migration in earthquake swarms. J. Volcanol. Geotherm. Res. 257, 159–173.
Miller, C.A., Williams-Jones, G., Fournier, D., Witter, J., 2016. 3D gravity inversion and thermodynamic modeling reveal properties of shallow silicic magma reservoir beneath Laguna del Maule, Chile. Earth Planet. Sci. Lett. 459, 14–27.
Miller, C.A., Le Mével, H., Currenti, G., Williams-Jones, G., Tikoff, B., 2017. Microgravity changes at the Laguna del Maule volcanic field: magma-induced stress changes facilitate mass addition. J. Geophys. Res. Solid Earth 122. https://doi.org/10.1002/2017JB014048.
Poupinet, G., Ellsworth, W.L., Frechet, J., 1984. Monitoring Velocity Variations in the Crust Using Earthquake Doublets: An Application to the Calaveras Fault, California. 386. USGS Staff — Published Research.
Richardson, J., Waite, G., 2013. Waveform inversion of shallow repetitive long period events at Villarrica Volcano, Chile. J. Geophys. Res. Solid Earth 118:4922–4936. https://doi.org/10.1002/jgrb.50354.
Riley, P., Tikoff, B., Hildreth, W., 2012. Transtensional deformation and structural control of contiguous but independent magmatic systems: Mono-Inyo Craters, Mammoth Mountain, and Long Valley Caldera, California. Geosphere 8:740–751. https://doi.org/10.1130/GES00662.1.
Riller, U., Petrinovic, I., Ramelow, J., Strecker, M., Oncken, O., 2001. Late Cenozoic tectonism, collapse caldera and plateau formation in the central Andes. Earth Planet. Sci. Lett. 188 (3–4), 299–311.
Saxby, J., Gottsmann, J., Cashman, K., Gutiérrez, E., 2016. Magma storage in a strike-slip caldera. Nat. Commun. 7:12295. https://doi.org/10.1038/ncomms12295 http://www.nature.com/doifinder/10.1038/ncomms12295.
Shelly, D.R., Beroza, G.C., Ide, S., 2007. Non-volcanic tremor and low frequency earthquake swarms. Nature 446:305–307. https://doi.org/10.1038/nature05666.
Shelly, D.R., Hill, D.P., Massin, F., Farrell, J., Smith, R.B., Taira, T., 2013. A fluid-driven earthquake swarm on the margin of the Yellowstone caldera. J. Geophys. Res. Solid Earth 118:1–15. https://doi.org/10.1002/jgrb.50362.
Singer, B., Andersen, N., Le Mevel, H., Feigl, K., DeMets, C., Tikoff, B., Thurber, C., Jicha, B., Cardona, C., Cordova, L., Gil, F., Unsworth, M., Williams-Jones, G., Miller, C., Fierstein, J., Hildreth, W., Vazquez, J., 2014. Dynamics of a large, restless, rhy-olitic magma system at Laguna del Maule, southern Andes, Chile. GSA Today. 24: pp. 4–10. https://doi.org/10.1130/GSATG216A.1.
Snoke, J.A., Munsey, J.W., Teague, A.C., Bollinger, G.A., 1984. A program for focal mechanism determination by combined use of polarity and SV-P amplitude ratio data, Earthq. Notes 55 (3), 15.
Spinks, K., Acocella, V., Cole, J., Bassett, K., 2005. Structural control of volcanism and caldera development in the transtensional Taupo Volcanic Zone, New Zealand. J. Volcanol. Geotherm. Res. 144, 7–22.
Thurber, C.H., 1983. Earthquake locations and three-dimensional crustal structure in the Coyote Lake area, central California. J. Geophys. Res. 88, 8226–8236.
Waldhauser, F., Ellsworth, W.L., 2000. A double-difference earth-quake location algorithm: method and application to the northern Hay-ward fault. Bull. Seismol. Soc. Am. 90, 1353–1368.
Walter, T.R., 2007. How a tectonic earthquake may wake up volcanoes: stress transfer during the 1996 earthquake–eruption sequence at the Karymsky Volcanic Group, Kamchatka. Earth Planet. Sci. Lett. 264 (2007), 347–359.